Thermal and Morphological Studies on γ-Fe_2O_3 Polystyrene Composites and the Affect of Additives

B. Govindaraj,[1] N. V. Sastry,[2] A. Venkataraman[3]*

[1]*Department of Chemistry, Vijayanagar College, Hospet 583 201, India*
[2]*Department of Chemistry, Sardar Patel University, Vallabh Vidyanagar 388120 Gujarat, India*
[3]**Department of Chemistry, Gulbarga University, Gulbarga 585 106, India*

Received 11 June 2003; accepted 22 December 2004
DOI 10.1002/app.20425
Published online in Wiley InterScience (www.interscience.wiley.com).

ABSTRACT: γ-Fe_2O_3polystyrene (PS) composite films were prepared by a gel-casting technique to obtain monodisperse composite films. To understand the effect of additives on the prepared composite films, additives such as rice husk ash and thiourea were made to disperse into the PS matrix. The as-prepared γ-Fe_2O_3 PS composite films, along with their additives, were subjected to characterization and study by X-ray diffraction, scanning electron microscopy, thermal, IR, and dielectric measurement techniques. These studies showed monodisperse and chemically homogenous composite films with an increase in thermal behavior. An interesting self-assembly of rod-like nanoparticles of γ-Fe_2O_3 particles into the polymer matrix, which formed spherical packets, was observed for the γ-Fe_2O_3PS composite film. The electrical behavior of these films was interesting, as some showed conduction whereas others showed an increase in dielectric behavior. This nature was explained by the dielectric measurements. © 2004 Wiley Periodicals, Inc. J Appl Polym Sci 93: 778–788, 2004

Key words: magnetic polymers; composites; additives; morphology; structure

INTRODUCTION

Maghemite (γ-Fe_2O_3) is a technologically important compound widely used for the production of magnetic materials and catalysts.[1,2] Maghemite nanoparticles exhibit superparamagnetic behavior because of a small coercivity arising from a negligible energy barrier in the hysteresis of the magnetization loop.[2–4] They have recently attracted considerable interest as optical–magnetic media in magneto-optical devices. Optical–magnetic media can be made by the deposition of magnetic and optically transparent particles inside supporting transparent materials, and maghemite nanoparticles satisfy these requirements because they can be easily incorporated into ultrathin polymer films.[5–8]

A nanocomposite is a material composed of two or more phases, one of which has a grain size of less than 100 nm. Here the combination of different physical and chemical properties leads to the formation of novel materials. Research is being conducted on the preparation of these nanomaterials with particle sizes from 100 nm down to less than 10 nm. The pioneering work of Gleiter and coworkers,[9] and that of many other research groups have contributed to synthesis[2,10–13] and properties[2,14–17] of nanomaterials and the nanocomposites. Several methods of synthesis, such as inert gas condensation,[10] the sol–gel process, and microwave plasma processing involving reactions at interfaces, have been developed to obtain novel nanomaterials in bulk and film form.[2,5,12,16]

When carbon and other additives are dispersed in polystyrene (PS) and other polymer matrices, the properties (e.g., thermal, structural) change markedly.[17–20] In this study, the amorphous carbon obtained from processed rice husk ash (RHA) was used as an important nonmagnetic additive. This study helped us to understand processing of the polymer composite and the structural–microstructural changes occurring in these composites. The effects of an organic ligand, such as thiourea, when complexed to the polymer helped clarify the advantages of adding such additives.

EXPERIMENTAL

γ-Fe_2O_3 was obtained from a ferrous succinate tetrahydrate precursor by a self-propagating combustion reaction.[21,22] The as-prepared γ-Fe_2O_3 was characterized for its structure, thermal properties, and morphology. Monophasic γ-Fe_2O_3 was obtained, as seen from the X-ray diffraction (XRD) pattern, which is discussed later. The morphology of this material

Correspondence to: A. Venkataraman (venkat95@sancharnet.in).

Contract grant sponsor: University Grants Commission (UGC), Kamataka University, Dharwad, India (to B.G.).

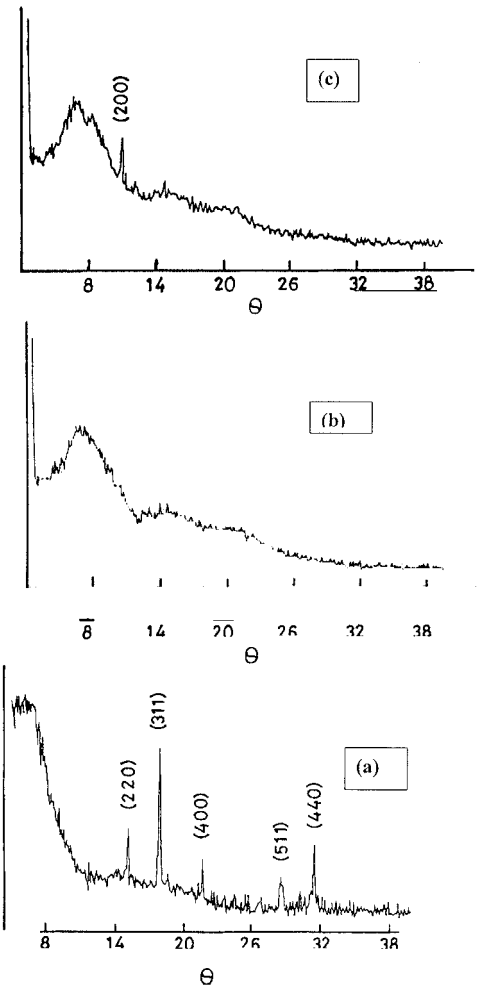

Figure 1 XRD patterns of (a) γ-Fe_2O_3, (b) the PS film, and (c) the PSG composite film. The *y* axis represents relative intensity in all parts of the figure.

showed the presence of nanosized spherical particles and agglomerates ranging between the submicron level to 10 μm. These particles possed different shapes and sizes along with some agglomerates closely packed together. The IR spectrum of this material showed two absorption peaks characteristic of ferrite. The structure, spectroscopic, and thermal characterizations are reported elsewhere.[21]

Characterization techniques

The XRD patterns are obtained with a Seimens X-ray diffractometer (Japan), and the target used was CuK_α (λ = 1.54 Å). The X-ray generator was operated as 30 kV and with a 20 mA current. The scanning range (θ) was selected. A scanning speed of 1° min and a chart speed of 20 mm/min were used for the precise determination of the lattice parameters. High-purity silicon powder was used as an internal standard.

The scanning electron microscopy (SEM) images of the samples were obtained with a Leica-440 Cambridge steroscan scanning electron microscope. The scanning electron microscope was operated at 20 kV. The samples were made conducting by the sputtering of gold with a Poloron direct-current sputtering unit, operated at 1.4 kV and with a 18–20mA current. The SEM images were taken with OROW 35-mm film.

The IR spectra of the samples were recorded on a PerkinElmer Fourier transform infrared spectrometer (model 1000) in the range 300–4000 cm^{-1}.

Thermal data was obtained from Mettlar Toledo Star instruments (Weinheim, Germany) under a dynamic flow of nitrogen at a flow rate of 100mL/min and a heating rate of 10°C/min.

The experimental setup to measure dielectric properties consisted of a capacitance bridge (General Radio type 1615 A; Princeton, NJ) with a three-terminal network and a crystal assembly holder. The details were reported elsewhere.[23]

Preparation of the γ-Fe_2O_3 thiourea complex (TUG) composites

A know weight of thiourea was dissolved in acetone, and to this solution, an equal quantity of γ-Fe_2O_3 was added. Then, the resulting γ-Fe_2O_3 dispersed mixture was added into a round-bottom flask and refluxed on a water bath (maintained at 35°C) for about 6 h. After refluxing, the solvent was slowly evaporated on a temperature-controlled hot plate. The final dried powder product was collected and characterized with IR and SEM techniques, and the sample was used as

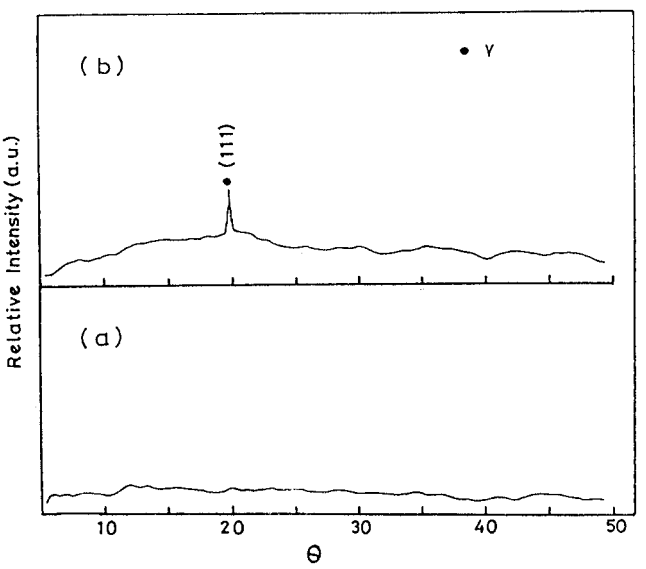

Figure 2 XRD patterns of (a) RHA and (b) the PSGA composite film.

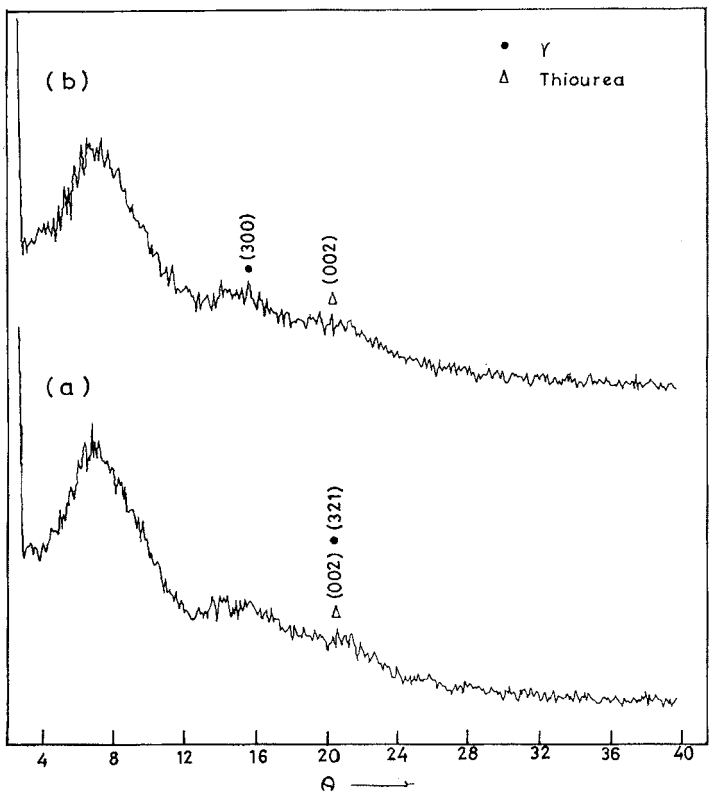

Figure 3 XRD patterns of (a) the PSTUG composite film and (b) the PSTUGA composite film. The *y* axis represents relative intensity.

adsorbent for the adsorption study. The characterization of this sample was reported elsewhere.[21]

Preparation of γ-Fe_2O_3 polymer composites

PS was obtained from M/S Supreme Petrochemicals (Mumbai, India).

Preparation of γ-Fe_2O_3 polystyrene composite films

PS (1 g) was dissolved in 50 mL of the solvent xylene. To this solution, 0.1 g (10 wt %) of the as-prepared γ-Fe_2O_3 was added, and the dispersion sol was then transferred to vacuum rotary evaporator and sonicated (so that there was no formation of agglomerates and so that the films possessed uniform dispersion) for 0.5 h. The solutions were mixed in a rotary evaporator that was constantly maintained at 60–80°C. The solvent was evaporated slowly by the application of a vacuum. A uniform γ-Fe_2O_3, dispersed PS film was obtained. The same procedure was repeated with varying weight percentages of 2 and 5 (0.02 and 0.5 g of γ-Fe_2O_3).

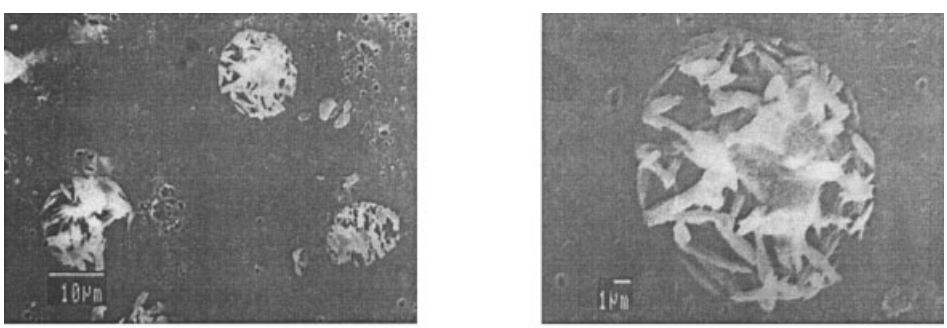

Figure 4 SEM images of the PSG composite film at (a) low and (b) high magnification.

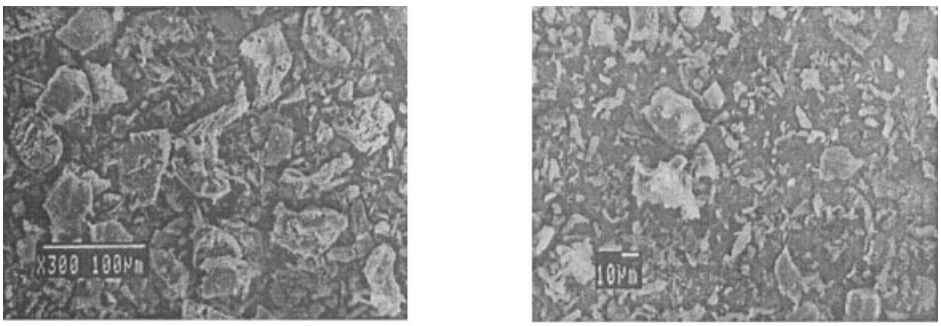

Figure 5 SEM images of processed RHA at (a) low and (b) high magnification.

Preparation of processed RHA

Rice husk from the local rice mill was treated with nitric acid with constant stirring. The mixture was kept for 24 h to remove excess oxides and impurities from the husk. Then, the mixture was filtered, washed with distillate water, and dried. This treated husk was finely grounded and ignited in a silica crucible kept in an electric oven at 600°C. A pale white powder was obtained after 2 h. Heating and weighing was repeated for a constant weight. This powdered RHA was used as one of the nonmagnetic additives added into polymer, and the composite was studied through various techniques.

Preparation of γ-Fe_2O_3 polymer composite films with additives

To study the effect of nonmagnetic additives such as RHA and thiourea, the polymer composite films were prepared with PS and RHA and the TUG complex separately.

The as-prepared γ-Fe_2O_3 sample was made to disperse in the PS gel obtained by the dissolution of the polymer in the solvent xylene. The dispersed γ-Fe_2O_3 sample in the PS matrix was taken out as a thin film (PSG) through a gel-casting technique. Similarly, chemically treated RHA was also dispersed in the PS matrix and obtained as a film (PSA). A mixture of RHA and γ-Fe_2O_3 at a ratio of 1:1 by weight was also dispersed in the PS matrix to obtain a film (PSGA). TUG was prepared by the refluxing of the mixture of thiourea and γ-Fe_2O_3 at a weight ratio of 1:1. The as-prepared TUG was made to disperse into the PS matrix, and the film PSTUG was obtained by a gel-casting technique. Similarly, the 1:1 mixture of TUG and RHA was made to disperse into the PS matrix to obtain the PSTUGA film by the same gel-casting technique. In this way, the composite films with additives (2, 5, and 10 wt %) were prepared. Among these films, the detailed characterization and study for the composite film of PS with 10 wt % of the additives is reported in this article, as a uniform dispersion of the additives in this composite film was observed.

The as-prepared PS composite films were subjected to characterization and studies, wherein the similarities were observed; only the representative figures and data are presented in this article.

RESULTS AND DISCUSSION

XRD

The XRD pattern of γ-Fe_2O_3, PS, film, and PSG composite films are shown in Figure 1(a–c). The compar-

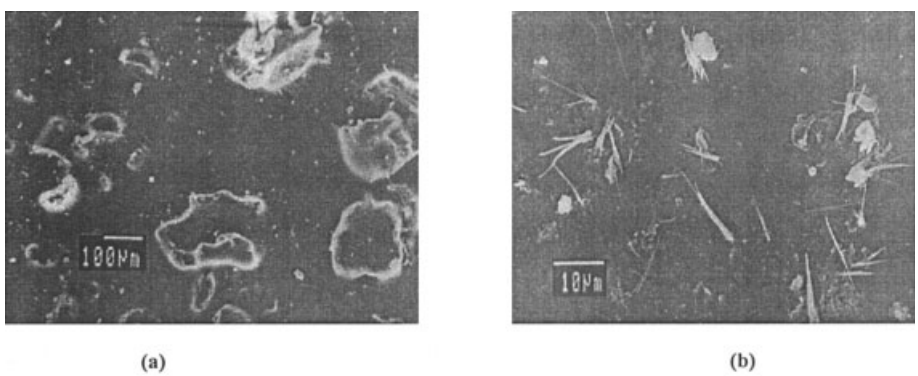

Figure 6 SEM images of the PSA composite film at (a) low and (b) high magnification.

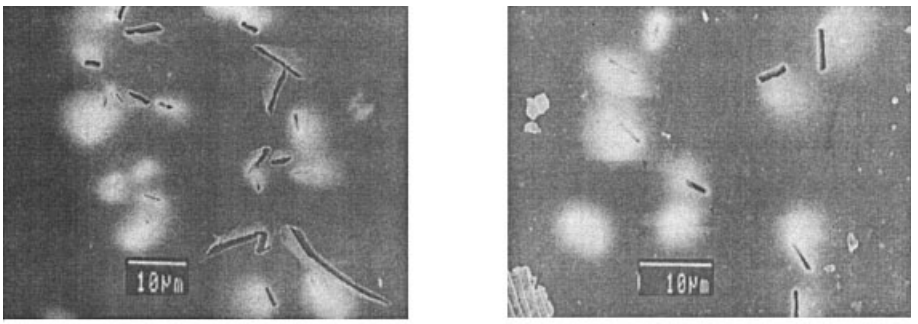

Figure 7 SEM images of the PSTUG composite film at (a) low and (b) high magnification.

ison of these XRD traces showed that γ-Fe_2O_3 particles were ultrafine with crystallite sizes of around 80 nm, as obtained from the line broadening of the X-ray profile with Scherrer formulae, whereas PS film is amorphous in its nature. However, the composite film PSG showed some crystalline phase due to the dispersion of γ-Fe_2O_3 particles in the PS matrix. Figure 1(c) shows a peak at the *d* value of 4.0613 Å corresponding to a Miller index of (200, ASTM 4–755). However, the other Miller indices of γ-Fe_2O_3 were masked by the PS matrix. These observations infered that the γ-Fe_2O_3 particles observed as spherical packets in the SEM images (dealt with later in this article) may have been crystalline in nature.

Figure 2(a,b) shows the XRD patterns of processed RHA and the polymer composite PSGA. XRD of RHA showed an amorphous nature [Fig. 2(a)] and XRD of PSGA showed a maximum portion of its nature as amorphous along with a slight crystallinity, possibly due to the presence of γ-Fe_2O_3 particles. A peak at the θ value of 20° was assigned for γ-Fe_2O_3 with the Miller index of (111). This observation was in accordance with the reported results (ASTM file no. 4–755).

The XRD patterns of PSTUG and PSTUGA are shown in Figure 3(a,b). In both of these patterns, the amorphous nature of PS can be observed along with some crystallinity because of the presence of thiourea. Both of the patterns have a small peak at a θ value of 20.73°, which was assigned to thiourea with a Miller index of (002) and γ-Fe_2O_3 with a Miller index of (321). This showed that the complex composite thiourea with γ-Fe_2O_3 showed crystallinity in its nature and was homogeneously dispersed in the PS matrix. The presence of RHA as amorphous in its nature showed no significance in the XRD pattern [Fig. 3(b)]. However, in this figure, the γ-Fe_2O_3 peak was shifted to a θ value 15.75° with a Miller index of (300). All of these observations were in accordance with ASTM file numbers 03-0235 (for thiourea) and 4–755 (for γ-Fe_2O_3).

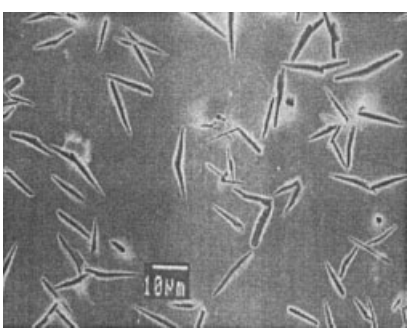

Figure 8 SEM image of the PSTUGA composite film.

SEM

The SEM images of PSG with low and high magnifications are shown in Figure 4(a,b). Figure 4(a) shows the self-assembled rod-like spherical packets of γ-Fe_2O_3 particles observed in the polymer matrix. Figure 4(b) shows that the ultrafine grains of γ-Fe_2O_3 were modified to a rod-shaped knitted giant structure. This may have been due to the accumulation of γ-Fe_2O_3 particles as spherical packets. The SEM images of RHA are shown in Figure 5 (a,b) with low and high magnifications. As shown in this figure, the particles of RHA possesed different sizes and shapes. The particle size of the RHA was in the range of 1–50 μm.

The SEM images of PSA are shown in Figure 6(a,b) with low and high magnifications. The SEM images show spherical and needle-shaped ash particles uniformly dispersed in the PS matrix.

The SEM images of PSTUG (TUG complex dispersed in the PS matrix) are shown in Figure 7(a,b) with low and high magnifications. These figures show the needle-shaped thiourea particles dispersed in the PS matrix. The charging is due to the possible presence of thiourea particles dispersed in the PS. The thiourea particles were randomly oriented. The presence of γ-Fe_2O_3 in the polymer matrix could not be clearly identified.

The SEM image of PSTUGA is shown in Figure 8. Shown in Figure 8 is the combination of spherical-shaped ash particles and needle-shaped thiourea particles randomly dispersed in the PS matrix. The particles were arranged in a closer fashion than earlier

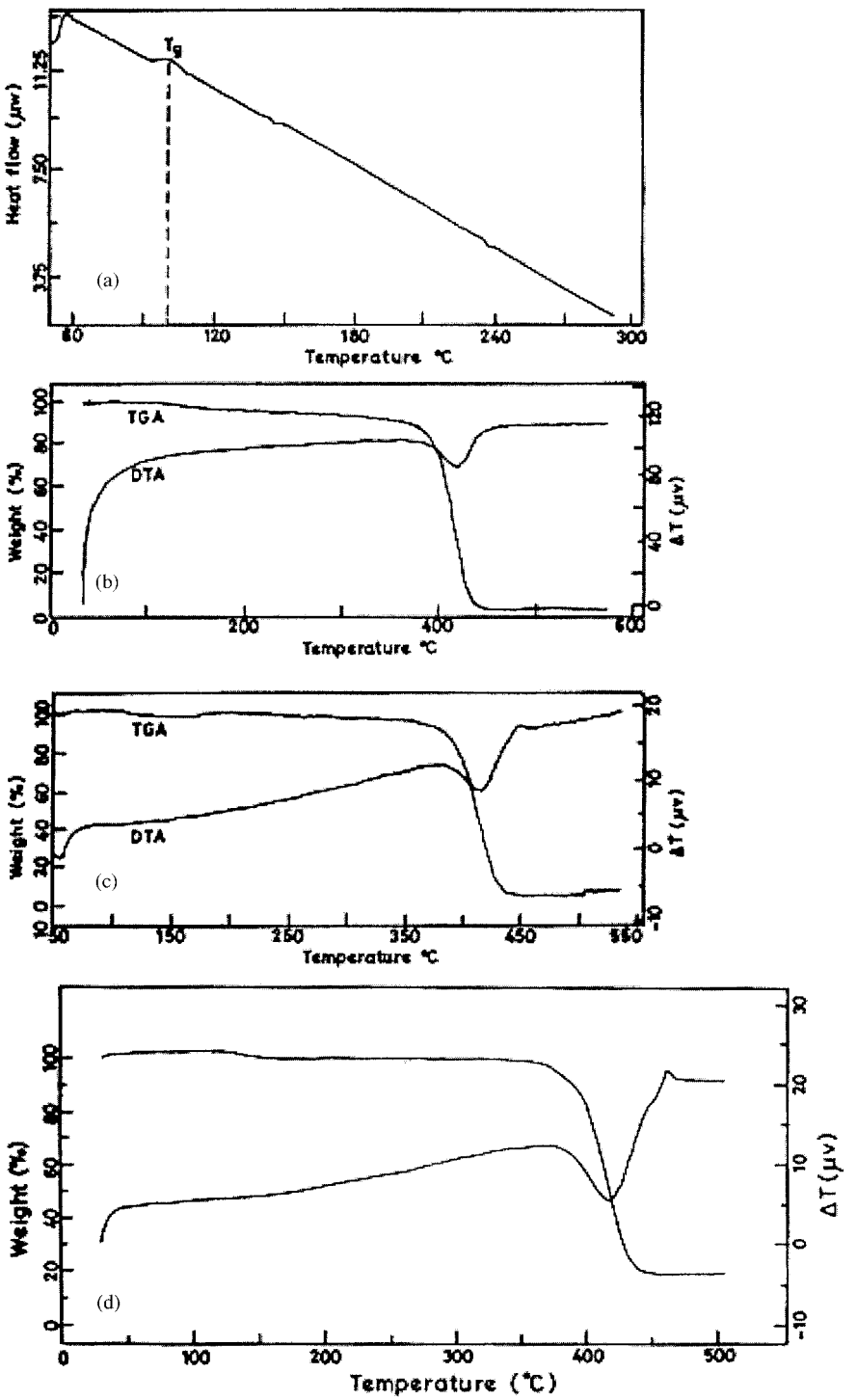

Figure 9 (a) DSC trace of the PS film, (b) TGA/DTA trace of the PS film, (c) TGA/DTA trace of the PSG composite film, and (d) TGA/DTA trace of the PSTUGA composite film.

ones. The presence of γ-Fe_2O_3 in the matrix could not be clearly observed in this case.

Thermal study

Figure 9(a) shows the differential scanning calorimetry (DSC) trace of the PS film; Figure 9(b) shows the thermo gravimetric analysis(TGA)/differential thermal analysis (DTA) trace of the PS film, and Figure 9(c) shows the TGA/DTA traces of the PSG composite film. These thermal traces were obtained under nitrogen atmosphere at a heating rate of 10°C/min and a flow rate of 100 mL/min. A comparison of these figures clearly indicated that the thermal stability of the PSG composite film slightly increased compared to

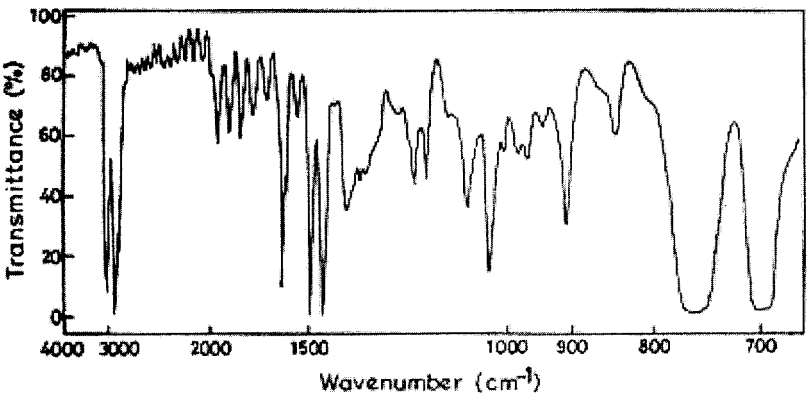

Figure 10 IR spectrum of the PS film.

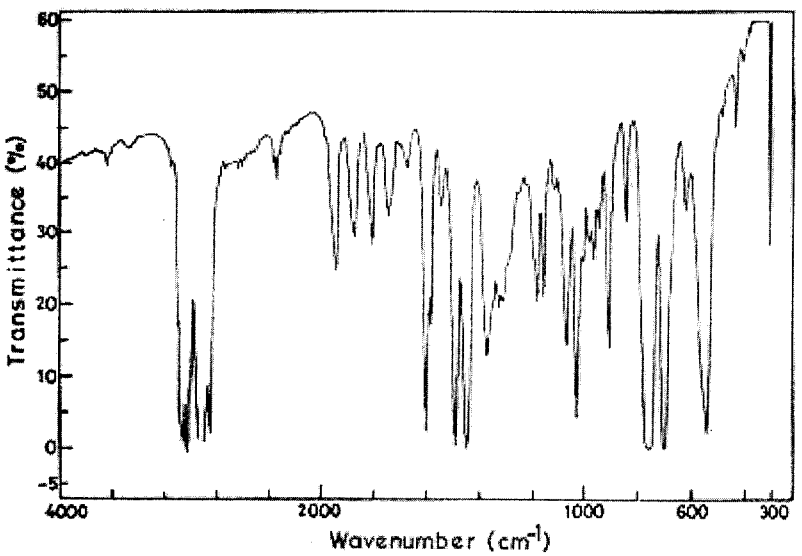

Figure 11 IR spectrum of the PSG composite film.

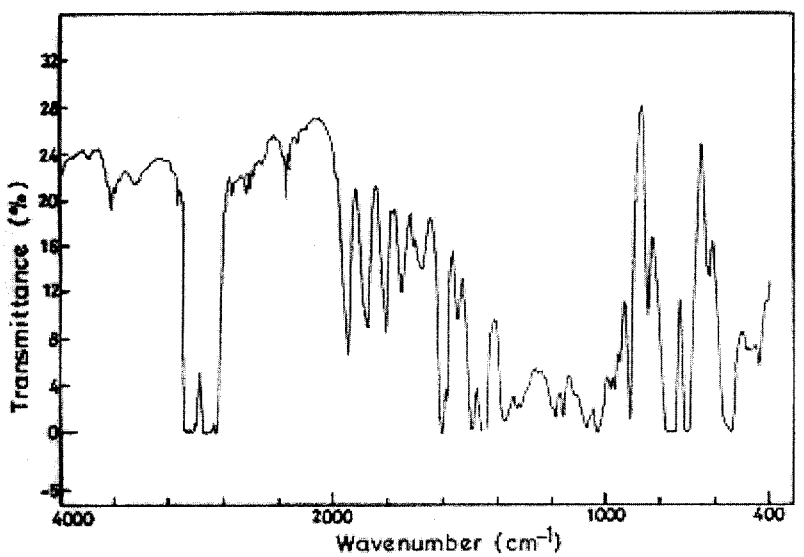

Figure 12 IR spectrum of the PSA composite film.

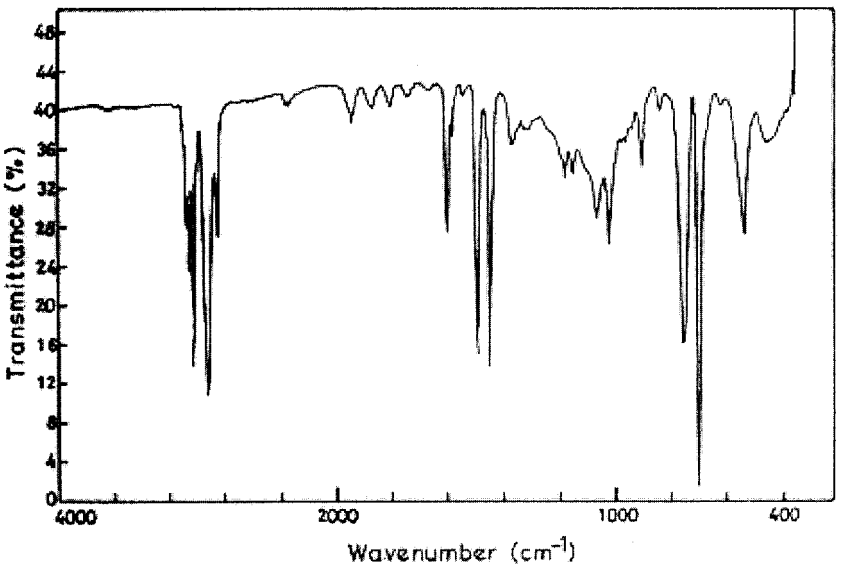

Figure 13 IR spectrum of the PSGA composite film.

that of the pure PS film. The DSC trace showed the glass-transition temperature (T_g) for PS around 100°C. As indicated by the DTA traces in Figure 9 (b,c), the polymer degradation occured around 418°C. The TGA traces in Figure 9 (b,c) showed a smooth, single-step weight loss, indicating a pattern of decomposition of the polymer and polymer composites to behave similarly. The DTA and TGA traces also indicated that the composite film PSG had some adsorbed water molecules. The TGA traces showed the formation of some char after decomposition for both pure PS and the composite films. These observations confirmed the fact that the PS composites showed better processibility.

Figure 9(d) shows the TGA/DTA trace of PSTUGA. The TGA trace showed a step I weight loss of 0.6% in the temperature range 45–224°C. Then, the TGA trace showed the thermal stability of PSTUGA up to 380°C with a weight loss of merely 4.9% from 224 to 380°C (step II). Then, a single step of continuous weight loss occurred from 380 to 437°C (step III), where a weight loss up to 72.8% was observed. This was followed by the last step (step IV), which was again a slow process, showing 2.2% weight loss from 437 to 493°C. At 493°C, a residue of 19.5% was obtained. This residue may have involved Fe_2O_3, char and possibly FeS as a mixture. However, the residue could not be analyzed for the exact composition of its components. The endothermic peaks on the DTA trace at 416 and 468°C supplemented the TGA results.

IR spectroscopic study

An IR spectral investigation of the composites PSG, PSA, and PSGA were undertaken and are reported here. These spectra were compared with the IR spec-

TABLE I
Comparison of IR Absorption Peaks of PS and Its Composite Films

PS (cm^{-1})	PSG (cm^{-1})	PSA (cm^{-1})	PSGA (cm^{-1})
3050	3648	3648	3626
2900	3081	3473	3444
2650	3060	3024	3055
2350	3026	2919	2896
2250	2919	2854	2333
2200	2850	2337	1944
2150	2337	1943	1869
2050	1943	1871	1798
1950	1871	1803	1739
1875	1803	1745	1641
1850	1743	1669	1596
1750	1669	1601	1450
1675	1601	1542	1146
1625	1583	1492	837
1550	1542	1450	770
1500	1492	1373	699
1450	1451	1181	568
1375	1373	1154	
1325	1328	1070	
1225	1181	1028	
1185	1154	907	
1160	1069	841	
1115	1028	747	
1060	980	704	
1040	964	621	
1010	942	541	
980	906	435	
960	842		
945	757		
910	700		
845	621		
760	540		
700	435		
	405		
	308		

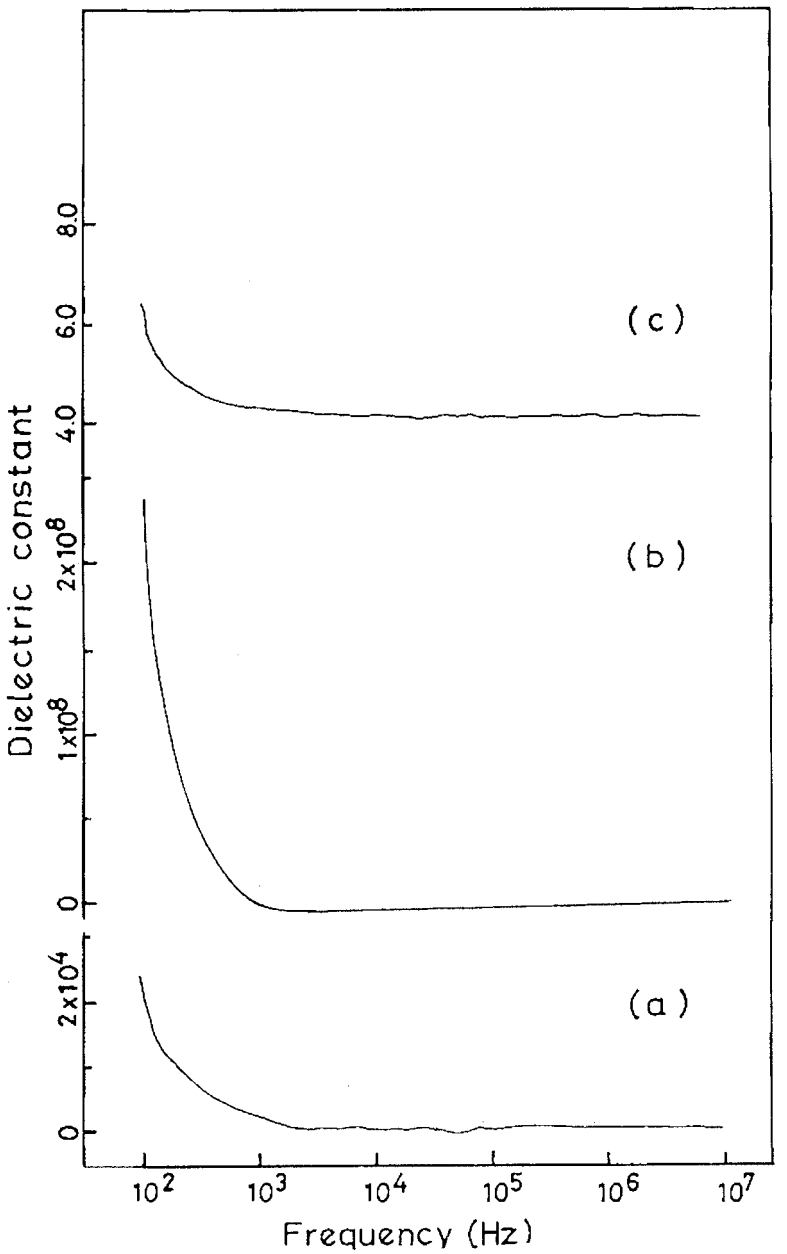

Figure 14 Dielectric constant measurements of (a) the PS film, (b) the PSTUG composite film, and (c) the PSTUGA composite film.

trum of pure PS. The IR spectrum of standard PS is shown in Figure 10. The IR spectra of the PS composite films are shown in Figures 11–13, and the comparison of IR absorption peaks of these composites with pure PS is given in Table I.

The IR spectrum of PSG is shown in Figure 11. On comparison of this spectrum with that of pure PS (Fig. 10), we observed that PSG had extra peaks at 621, 540, 435, 405, and 308 cm^{-1}. This was due to the presence of γ-Fe_2O_3 in the polymer matrix. These vibrations (540, 435, and 405 cm^{-1}) are characteristic of a Fe—O vibrational mode of frequencies. Other peaks resembled the PS spectrum with some shift because of complex formation with γ-Fe_2O_3 dispersed in the PS matrix.

The IR spectrum of PSA is shown in Figure 12. On comparison of this figure with that of pure PS (Fig. 10), we observed that some new peaks emerged in the PSA sample, whereas some peaks disappeared that were present in PS. The peaks at 1200–800 cm^{-1} pertained to a C—C stretching mode. These were characteristic of the presence of ash in the PS matrix. The other peak at 435 cm^{-1} was due to the C—C bending mode. The extra peak at 1070 cm^{-1} gave us confirmation for the C—C stretching mode of ash. The extra peak at 3473 cm^{-1}, which was not present for PS, may have been due to the presence of moisture.

The IR spectrum of PSGA is shown in Figure 13. On comparison of this figure with PS, PSG, and PSA, we

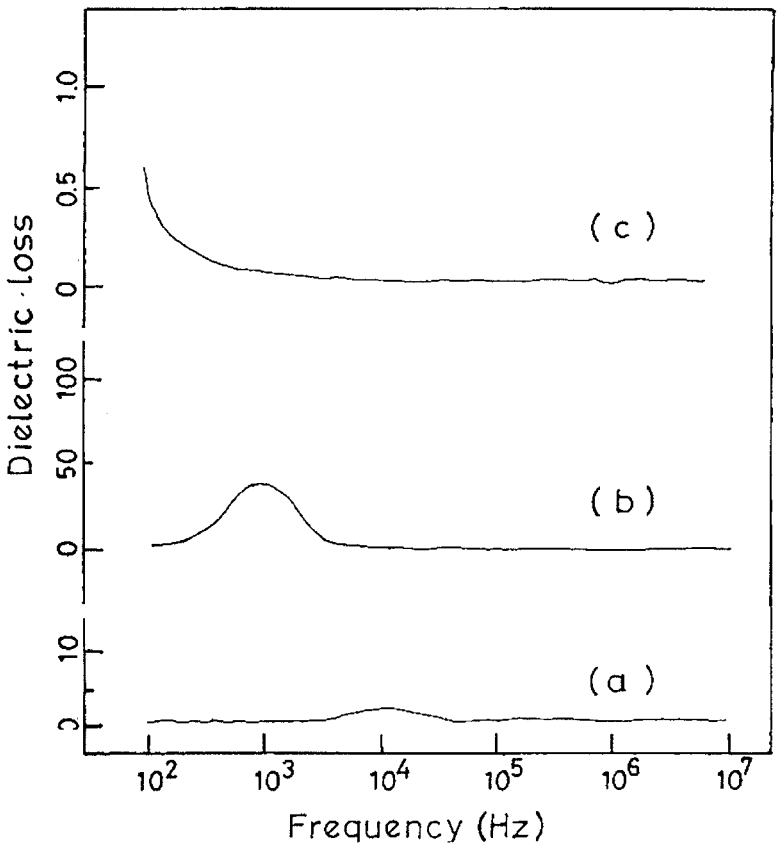

Figure 15 Dielectric loss behavior of (a) the PS film, (b) the PSTUG composite film, and (c) the PSTUGA composite film.

observed that the combination of PSG and PSA constituted this figure with a remarkable change in absorption in the frequency range around 1200–800 cm^{-1}. All of the peaks pertaining to the C—C stretching mode completely disappeared. The γ-Fe_2O_3 peaks also shifted, indicating a possible complex composite formation of γ-Fe_2O_3 and ash with the PS matrix.

Overall, the IR study of these PS composites revealed that the appearance of new peaks other than those of the constituent materials of PS and γ-Fe_2O_3, and along with the changes in existing peaks or the disappearance in the IR spectra clearly indicated the complexation of γ-Fe_2O_3 and ash with the PS matrix. However, the nature of bonding could not be understood, as PSA and PSG had the same peaks in the metal–oxygen (M—O) range, which overlapped with C—C bending in ash. The identification of the exact nature of bonding is beyond the scope of this investigation.

Dielectric study

Figure 14(a–c) shows the variation in the dielectric constant with respect to frequency (up to 10 GHz) for the PS, PSTUG, and PSTUGA samples. The PSG and PSGA samples showed conducting behavior, and hence, a dielectric study could not be undertaken. Figure 14(a) shows the dielectric constant for PS with an exponential decrease in the dielectric constant, which reached zero at about 5×10^3 Hz. Thereafter, the dielectric constant remained the same throughout.

Figure 14(b) shows the dielectric constant for PSTUG with an exponential decrease in the dielectric constant, which reached zero at about 1×10^3 Hz. Thereafter, the dielectric constant remained the same throughout.

Figure 14(c) shows the dielectric constant behavior for PSTUGA. For the TUG complex, along with ash, when added into the PS matrix, the dielectric behavior of the PSTUGA composite showed a slow and gradual decrease in the dielectric constant, which reached a value of about 5 at a frequency of 8×10^3 Hz. Thereafter, the dielectric constant remained almost the same.

We understand from this study that the incorporation of ash and γ-Fe_2O_3 into the PS matrix resulted in a loss of dielectric behavior. However, the incorporation of an organic ligand, such as the TUG complex, increased the dielectric polarization, resulting in a higher dielectric constant. These observations were supplemented by the study of dielectric loss versus frequency, as shown in Figure 15(a–c) for the PS, PSTUG, and PSTUGA composite samples.

Figure 15(a) shows a weak peak (indicating an increase and decrease in loss) from 1×10^3 to 4×10^4 Hz, which remained almost zero later. Figure 15(b) shows a similar loss but with higher intensity peak in the frequency range 1×10^2 to 3×10^3 Hz. Figure 15(c) shows that the dielectric loss decreased drastically up to 10^3 Hz and, thereafter, remained zero. This loss behavior was in agreement with the dielectric constant observations made for the composite samples.

CONCLUSIONS

1. The composite films showed partial crystallinity, indicating the masking of some of the Miller planes of the ceramic materials by the polymer matrix.
2. The IR spectra for these films showed several vibrational bands at various wave numbers. Similarity was observed with the addition of additives. Several new bands disappeared in the IR spectra of the composite films due to the formation of complexes by the addition of γ-Fe_2O_3 to the PS matrix.
3. SEM images of the PS-*g*-Fe_2O_3 composite showed the particle morphology of γ-Fe_2O_3 as self-assembly, rod-like particles embedded in spherical packets of the polymer matrix.
4. The thermal study showed an increase in the thermal stability of the composites compared with the pure polymer.
5. The dielectric study indicated a decreasing trend of dielectric constant with the addition of γ-Fe_2O_3 and ash to the PS matrix. However, with the addition of the organic ligand thiourea, the dielectric constant increased. The dielectric loss behavior was also in agreement with dielectric constant observations made for the composite samples. These composites may show potential applications as sensor materials, electromagnetic insulation (EMI) shields, and microwave absorbers.
6. The PS composite films were highly transparent, were best suitable for processing, and had an ease of fabrication because of their flexibility.

The authors are grateful to T. M. Aminabhavi (Director, University Grants Commission (UGC), Center of Excellence of Polymer Science, Karnataka University, Dharwad) for useful discussions and valuable suggestions.

References

1. Kryder, M. H. MRS Bull 1996, 21(9), 17.
2. Rao, C. N. R.; Kulkarni, G. U.; Thomas, P. J.; Agarwal, V. V.; Gautam, U. K.; Ghosh, M. Curr Sci 2003, 85, 1041.
3. Kroll, E.; Winnik, F. M.; Ziolo, R. Chem J Mater 1996, 8, 1594.
4. Tronc, E.; Prene, P.; Jolivet, J. P.; d'Orazio, F.; Lucari, F.; Fiorani, D.; Godinho, M.; Cherkaui, R.; Nogues, M.; Dormann, J. L. Hyperfine Interact 1995, 95, 129.
5. Fendler, J. H. Nanoparticles and Nanostructured Films Preparation, Characterisation and Applications; Wiley-VCH; Weinheim, Germany, 1998.
6. Ennas, G.; Musinu, A.; Piccaluga, G.; Zedda, D.; Gatteschi, D.; Sangregorio, C.; Stanger, J. L.; Concas, G.; Spano, G. Chem Mater 1998, 10, 495.
7. Tronc, E.; Jolivet, J. P.; Livage, J. Hyperfine Interact 1990, 54, 737.
8. Govindraj, B.; Sastry, N. V.; Venkataraman, A. J Appl Poly Sci, to appear.
9. Karch, J.; Birringer, R.; Gliter. H.; Nature 1987, 330, 556.
10. Kataby, G.; Prozorov, T.; Kolypin, Y.; Succenik, C. N.; Ulman, A.; Gedenken, A.; Langmuir 1997, 13, 6151.
11. Alivistos, A. P. Science 1996, 271, 933.
12. Pileni, M. P.; Nature Mater 2003, 2, 145.
13. Cornell, R. M.; Schwertmann, U.; The Iron Oxides: Structure, Properties, Reactions, Occurances and Uses; VCH; Weinheim, Germany, 1996.
14. Bahadur, P.; Sastry, N. V.; Riess, G. Colloids Surf 1987, 29, 343.
15. Diandre, L. P.; Ruben, D. R. Chem Mater 1996, 8, 1770.
16. Leslie-Pelecky, D. L.; Rieke, R. D. Chem Mater 1996, 8, 1770.
17. Mark, J. E. Curr Oppn Solid State Mater Sci 1999, 4, 529 (and references therein).
18. Ramachandran, J.; Vivekanandan, S. Lakshmi, S. Ind J Chem 2001, 40, 105.
19. Chen, A.; Wang, H.; Zhao, B.; Li, X. Synth Met 2003, 139, 411.
20. Barham, P. J. J Mater Sci 2000, 35, 5139.
21. Govindraj, B.; Venkataraman, A. Synth React Inorg Met-Org Chem, to appear.
22. Venkataraman, A.; Mukhedkar, V.A.; Rahaman, M.M.; Nikumbh, A.K.; Mukhedkar, A.J. Thermochim Acta 1987, 112, 231.
23. Hiremath, V.A. Venkataraman, A. Bull Mater Sci 2003, 26, 391.